Global Lightning Parameterization from CMIP5 Climate Model Output

BRIAN I. MAGI

Department of Geography and Earth Sciences, University of North Carolina at Charlotte, Charlotte, North Carolina

(Manuscript received 7 December 2013, in final form 15 October 2014)

ABSTRACT

Lightning is best known as a component of severe weather, but diverse communities of researchers, such as those in atmospheric chemistry and global fire modeling, have long recognized that lightning plays a significant role in many components of the Earth system. Global climate models are unlikely to be able to simulate lightning from first principles, but the same models do simulate many parameters related to convection, including total precipitation rate, convective precipitation rate, and convective mass flux. This study combines satellite observations of lightning and CMIP5 climate model simulations to derive an empirical parameterization of monthly lightning in terms of monthly simulated convective parameters. Convective mass flux best captures the spatiotemporal distribution of observed lightning. Derived lightning seasonality is captured with 95% confidence over 69% of land but only 30% of ocean. Spatially, the correlation of derived lightning and observed lightning is 0.74. Overall, global observations suggest lightning occurs at an annual rate of 47 flashes per second, while lightning from the parameterization occurs at 44 flashes per second. A robust feature of the relationship between lightning and climate model convective parameters is that lightning flash rate increases linearly with increases in convective precipitation rate and in convective mass flux for a significant subset of the total range of those convective parameters. Namely, this linear proportionality is evident when the convective precipitation rate is less than 4–5 mm day^{-1} and the convective mass flux is less than 15–16 kg m^{-2} h^{-1}, which account for about 90% of the values simulated by the climate models.

1. Introduction

Lightning affects nearly every part of the planet at varying times of the year. Global lightning flash rates derived from the optical transient detector (OTD) (Christian et al. 2003) and the lightning imaging sensor (LIS) (Boccippio et al. 2002; Mach et al. 2007), the latter of which is on the NASA Tropical Rainfall Measuring Mission (TRMM) (Kummerow et al. 2000) satellite, average 47 flashes per second (Cecil et al. 2014). About 4 times as much lightning occurs over land than over the oceans (e.g., Allen and Pickering 2002; Cecil et al. 2014), and distinct peaks in lightning activity occur over land in the deep tropics (Price 2009; Williams 2005). There is also a seasonal cycle in global lightning activity with a minimum in February and a maximum in August (Cecil et al. 2014).

In addition to an association with severe weather, lightning is energetic enough to play a role in atmospheric chemistry through the nitrogen biogeochemical cycle (e.g., Levy et al. 1996; Price et al. 1997; Shindell et al. 2006; Wu et al. 2008) and act as essentially the only significant natural ignition source for fires (Flannigan et al. 2009; Pechony and Shindell 2009; Price and Rind 1994). However, while lightning is an important phenomenon in the Earth system, global climate models do not directly simulate the process of lightning initiation and discharge (e.g., Tost et al. 2007). Atmospheric chemistry models, which are critical components of global climate models (e.g., Fiore et al. 2012), require lightning to simulate the natural formation of nitrogen oxides (Grewe et al. 2001; Price et al. 1997) and rely on climatologies of lightning from OTD/LIS or lightning parameterizations (Allen and Pickering 2002; Grewe et al. 2001; Wu et al. 2008). Global fire models rely on OTD/LIS climatologies (Kloster et al. 2010; Li et al. 2012; Pechony and Shindell 2009; Thonicke et al. 2010).

There are strengths and weaknesses in relying on either a climatology or a parameterization to incorporate lightning into a simulation framework. The OTD/LIS lightning climatology does not capture interannual variability, but it is accurate and completely based on

Corresponding author address: Brian Magi, Department of Geography and Earth Sciences, University of North Carolina at Charlotte, 9201 University City Blvd., Charlotte, NC 28223.
E-mail: brian.magi@uncc.edu

DOI: 10.1175/JTECH-D-13-00261.1

observations (Cecil et al. 2014). Lightning that is parameterized against observed cloud height (Price and Rind 1992), modeled convective mass fluxes, or convective precipitation (Allen and Pickering 2002; Barthe et al. 2010), or a combination of these (Grewe et al. 2001) is prone to large magnitude uncertainty in the number of lightning flashes or has poor ability to simulate the seasonality in lightning (Tost et al. 2007) when compared with OTD/LIS. There is therefore a disconnect between global models and reality in the sense that global models, especially global fire models, do not capture or even attempt to capture interannual variability or long-term secular changes in lightning distributions in response to modern or past climate changes.

Prior work has highlighted the relationship between lightning and other thunderstorm-related variables, such as convective precipitation (Petersen and Rutledge 1998; Petersen et al. 2005) and ice mass flux (Blyth et al. 2001; Deierling et al. 2005; Nesbitt et al. 2000). Theory and field studies (Blyth et al. 2001; Deierling et al. 2008) have repeatedly strengthened the idea that the noninductive charging process (Saunders et al. 1991; Takahashi 1978) is the dominant mechanism in cloud electrification that is sufficient to initiate lightning. This charging process involves collisions between larger ice hydrometeors (graupel) and smaller ice crystals in the presence of supercooled water (Blyth et al. 2001; Saunders et al. 1991).

Drawing from this physically based connection between lightning and convective properties related to ice and mass flux in thunderstorms, parameterizations of lightning activity for global modeling have been explored and discussed (Allen and Pickering 2002; Grewe et al. 2001; Price and Rind 1992; Tost et al. 2007). These and other parameterizations (e.g., Barthe et al. 2010) have been used as a basis for improving weather forecasting model simulations of regional precipitation (Papadopoulos et al. 2005; Pessi and Businger 2009; Tapia et al. 1998) and have been implemented in global chemistry models to study lightning-produced nitrogen oxides (Grewe et al. 2001; Levy et al. 1996; Shindell et al. 2006; Wu et al. 2008).

This study evaluates a global lightning parameterization based on a combination of observations and climate model output at relatively coarse spatiotemporal scales. Monthly lightning from OTD/LIS (Cecil et al. 2014) is used as the basis for developing an empirical relationship with monthly output from multiple climate models. The spatiotemporal scales of the global lightning parameterization in this study are well suited to applications in global modeling of chemistry, fires, and climate, and are easily adaptable to the particular model configuration. OTD/LIS data are used to evaluate the strengths and weaknesses of the lightning derived from the climate model output. The novel contribution of this work is that the parameterization is the first to connect global climate model output to the satellite-based global lightning climatology from OTD/LIS observations. No prior work has used multiple climate models to develop a lightning parameterization.

The datasets and methods used to test the consistency of observed and simulated convective parameters are presented in section 2, along with relevant descriptive statistics. In section 3, linear and nonlinear features of the relationship between lightning flash rate and the convective parameters are discussed to make the case for an empirical polynomial parameterization. The spatiotemporal distribution of present-day lightning activity derived from that parameterization and a robust linear feature in the relationship between observed lightning and climate model convective parameters are discussed in sections 3 and 4. Section 4 discusses strengths and weaknesses in the parameterization, and comparisons with a previous global lightning parameterization. Section 5 summarizes the results.

2. Methods

a. Datasets

Observations of lightning are from the global OTD/LIS high-resolution mean monthly climatology dataset (LISOTD_HRMC_V2.3, 0.5° × 0.5° spatial resolution) available online (http://thunder.nsstc.nasa.gov/; Cecil et al. 2014). OTD (available globally from 1995 to 2000) data are combined with LIS (available between 38°S and 38°N latitude from 1998 to the present) to create the monthly climatology used in this study, noting that the combined data product requires corrections to account for the lower sensitivity of OTD compared to LIS (Cecil et al. 2014). The overall OTD/LIS mean monthly climatology used in this study is based on lightning data from OTD and LIS from 1995 to 2012.

Observations of precipitation are from the monthly Global Precipitation Climatology Project (GPCP) version 2.2 (Adler et al. 2003; Huffman et al. 2009), which merges data from multiple satellite-based sensors and sounders with ground-based rain gauge data. The merged data product is available at 2.5° × 2.5° spatial resolution (at http://precip.gsfc.nasa.gov/). Error associated with the merged precipitation values are distributed as a part of the data product (Adler et al. 2003) and the mean error, weighted to precipitation, varies from 8% over land to 29% over the oceans. In this study, GPCP is used to evaluate whether climate models are capturing the spatiotemporal patterns in total precipitation.

TABLE 1. Climate models and datasets, the horizontal spatial resolution, and the globally averaged total precipitation, convective precipitation, and convective mass flux. Convective mass flux, as described in the text, is from the hybrid-sigma pressure level closest to 0.44, which is ~427 hPa. NCAR CCSM4 convective precipitation is not used in this study, but its average value is included, since total precipitation and convective mass flux are reasonable. More details about the individual climate models can be found on the CMIP5 website.

	Dataset or model name	Lat resolution (°)	Lon resolution (°)	Total precipitation (mm day^{-1})	Convective precipitation (mm day^{-1})	Convective mass flux (kg m^{-2} h^{-1})
—	OTD/LIS	0.50	0.50	—	—	—
—	GPCP version 2.2	2.50	2.50	2.69	—	—
1	MIROC5	1.41	1.41	3.21	1.49	8.61
2	BCC_CSM1.1	2.81	2.81	2.84	1.90	9.79
3	BCC_CSM1.1(m)	1.13	1.13	2.88	1.38	6.68
4	IPSL-CM5A-LR	1.88	3.75	2.73	1.32	4.78
5	IPSL-CM5B-LR	1.88	3.75	2.81	1.44	5.59
6	GFDL CM3	2.00	2.50	2.99	1.88	4.83
7	NCAR CCSM4	0.94	1.25	2.98	1.66×10^{-3}	9.01
8	INM-CM4.0	1.50	2.00	3.16	2.06	—
9	ACCESS1.3	1.24	1.88	3.16	1.84	—
10	CMCC-CM	0.75	0.75	2.90	1.46	—
11	GISS-E2-H	2.00	2.50	3.22	1.33	7.21
12	GISS-E2-R	2.00	2.50	3.18	1.31	6.88
13	HadGEM2-AO	1.24	1.88	3.10	2.27	—
14	FGOALS-g2.0	3.00	2.81	2.82	1.63	—
15	CNRM-CM5	1.41	1.41	3.06	2.48	—
16	CNRM-CM5.2	1.41	1.41	3.02	2.43	—
17	CSIRO Mk3.6.0	1.88	1.88	2.88	2.18	5.22
	Mean	1.67	2.09	3.00	1.78	6.86
	Std dev	0.60	0.87	0.16	0.41	1.80

Simulated total precipitation, convective precipitation, and convective mass flux are from climate models that contributed to the Coupled Model Intercomparison Project phase 5 (CMIP5, http://cmip-pcmdi.llnl.gov/cmip5/) data archive. CMIP5 (Taylor et al. 2012) is a coordinated effort among international climate modeling groups to simulate past, present, and future climate to better understand the response of the climate system to human and natural perturbations to energy balance. CMIP5 model output (Taylor et al. 2012) forms the basis for the Intergovernmental Panel on Climate Change Fifth Assessment Report (Stocker et al. 2013) Working Group reports.

The climate models used in this study are listed in Table 1 according to the CMIP5 protocol described online (http://cmip-pcmdi.llnl.gov/cmip5/terms.html), and with the model spatial resolution. Every climate model participating in CMIP5 archived precipitation as an output field, but only 17 climate models that archived both precipitation and convective precipitation fields were selected.

Of the 17 climate models, 10 also archived convective mass flux as a four-dimensional field—there is a vertical dimension, as well as the two horizontal dimensions and the time dimension. Convective mass flux is defined by CMIP5 as the net upward convective mass flux at a particular pressure level in the model and represents the difference between the updraft and downdraft mass fluxes. For this study, the convective mass flux at the closest hybrid-sigma pressure level to 0.44 is used. This value serves as an indicator of deep convection (Allen and Pickering 2002). The individual climate models have varying numbers of pressure levels, so the physical value of the pressure varies, but on average is ~427 hPa. Globally averaged values of precipitation, convective precipitation, and convective mass flux for each climate model and applicable dataset are listed in Table 1.

The climate model spatial grid (Table 1) is used when comparisons against that climate model are made. Thus, GPCP and OTD/LIS data are spatially interpolated to the model grid (Table 1). Additionally, the land and ocean masks particular to the individual climate model grids and available from CMIP5 are applied to the datasets to investigate land–ocean dependencies. In this study, an ocean grid cell is defined as a grid cell with land fraction equal to zero, while land grid cells are defined as any grid cell with land fraction greater than zero.

The time period of analysis for this study is 1995–2005, limited partly by OTD/LIS and partly by time bounds on CMIP5 experiments. Both the OTD/LIS and CMIP5 climate model output are compared using the mean monthly values, since climate models do not generally capture year-to-year variability in mesoscale meteorology. The start year is chosen because OTD/LIS climatology is based on a combination of OTD data available

from 1995 to 2000 and LIS data available from 1998 to the present (Cecil et al. 2014; Christian et al. 2003). The end year is chosen based on the final year of the CMIP5 "historical" model experiments (Taylor et al. 2012), which are compiled using observationally based emissions inventories (Lamarque et al. 2010) from the year 1850 to 2005. GPCP data are available from 1979 to the present (Adler et al. 2003; Huffman et al. 2009), but only data from 1995 to 2005 are used for any comparison. OTD/LIS mean monthly data are based on 1995–2012 and are not available for 1995–2005, but there is likely very little difference from mean monthly values from 1995 to 2005, since there were no significant changes to lightning distributions from 2006 to 2012 as compared to 1995–2005 (Cecil et al. 2014). The assumption is then that mean monthly OTD/LIS values from 1995 to 2012 are the same as mean monthly OTD/LIS values from 1995 to 2005.

b. Comparisons with precipitation observations

Comparison of mean annual total precipitation rate (MAP) from climate models against GPCP are shown in Fig. 1 for global, land-only, and ocean-only precipitation, with land and ocean grid cells defined in section 2a. This is a coarse-scale evaluation of model ability to simulate precipitation physics (e.g., Randall et al. 2007) in space, time, and magnitude.

As shown in Fig. 1, all the models are within 20% of the GPCP global MAP, and 7 of the 17 models are within 10%. Modeled MAP are, on average, biased high by 11% ($+0.31\,\mathrm{mm\,day^{-1}}$) compared to GPCP MAP. The agreement in global MAP (i.e., within 20%) is a combination of a low bias in land-based MAP and high bias in ocean-based MAP. On average, modeled land-based MAP are biased low by 11% ($-0.28\,\mathrm{mm\,day^{-1}}$) and modeled ocean-based MAP are biased high by 22% ($+0.63\,\mathrm{mm\,day^{-1}}$). Land-based MAP from eight climate models agree to within 10%, while the remaining climate models agree to within 30%. Ocean-based MAP from the 17 climate models agree to within 31% of GPCP ocean-based MAP. The high bias over the oceans and low bias over land act as compensating errors when examining global MAP, but the simulations of MAP are consistently more problematic (higher magnitude biases and percent differences) over the ocean.

In terms of the spatiotemporal comparison of global MAP from climate models compared to GPCP, Fig. 1 shows the time and space correlation coefficients. The spatial correlation is the linear correlation coefficient calculated by comparing the spatially explicit distribution of GPCP MAP with that of the individual climate models, where GPCP MAP is spatially interpolated to the climate model latitude–longitude grid (Table 1).

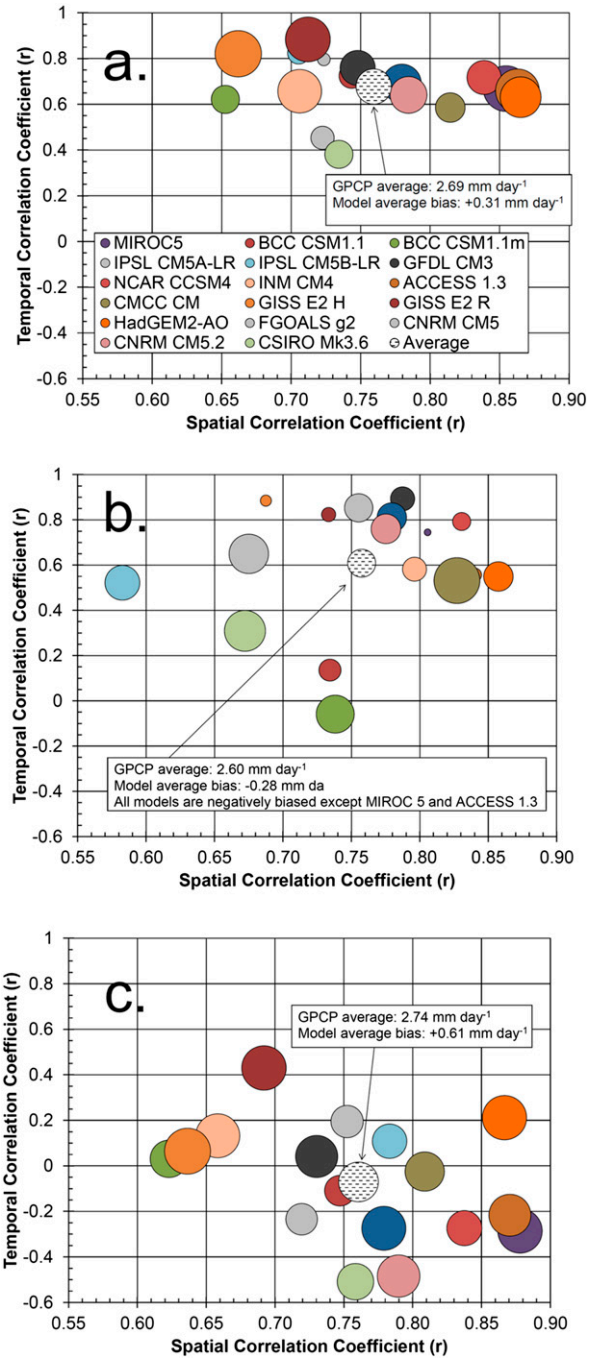

FIG. 1. Comparisons of observed precipitation rates from GPCP and simulated by CMIP5 climate models used in this study for (a) all grid cells, (b) land grid cells, and (c) ocean grid cells. The filled, colored circles each represent the absolute value of the difference between MAP rate from one of the climate models and GPCP: the larger the circle, the larger the difference from GPCP. The average difference is shown with a patterned fill, and the size of this circle is quantified in the inset. The spatial correlation is calculated from a comparison of the MAP from GPCP and from each climate model. The temporal correlation is calculated as a comparison of the mean monthly precipitation from GPCP and from each climate model. A near-perfect match to GPCP would have a very small circle diameter, and the circle would be located in the top-right quadrant.

Figure 1 suggests that, on average, about 58% of the spatial variability (i.e., mean of the squared linear correlation coefficient) of GPCP MAP is captured by models, with values ranging from 43% to 74%. Temporal correlation is the linear correlation coefficient calculated by comparing the 1995–2005 mean monthly time series (12 data points) from GPCP to those of the climate models. On average, about 47% of the seasonal variability of GPCP is captured, with climate models ranging from 15% to 70% of variability captured.

The same calculations of spatial and temporal correlations are made for land- and ocean-based MAP (Figs. 1b,c). Like global MAP, 58% of the spatial variability from GPCP is captured in land- and ocean-based MAP, suggesting that most of the modeled precipitation is simulated in the right place on Earth, regardless of land or ocean surface. However, ocean-based seasonal precipitation in the simulations captures only 7% of the variability suggested by GPCP compared to 44%–47% for the identical global and land-based comparisons.

To summarize Fig. 1, climate models, on average, capture a large fraction (>50%) of the global and land-based spatiotemporal patterns of precipitation when compared to GPCP, while magnitude comparisons suggest MAP is much better captured by climate models over land than over oceans. Simulations of ocean-based precipitation are weaker and, in terms of mean monthly seasonality, quite poor.

Evaluation of modeled precipitation has been discussed in detail by review studies (e.g., Meehl et al. 2012; Randall et al. 2007) and by individual model description studies (e.g., Donner et al. 2011; Dufresne et al. 2013; Gent et al. 2011; Wu et al. 2010). Part of the difficulty in accurately simulating precipitation in a global climate model is the sensitivity of precipitation to subgrid-scale convective dynamics (e.g., Donner et al. 2011; Tost et al. 2007). Other discrepancies arise as a result of the coupling of the ocean and atmosphere components of a climate model (e.g., Donner et al. 2011). A full analysis of physical reasons for strengths and weaknesses of individual or collective CMIP5 model simulations of precipitation, or uncertainties in GPCP (Adler et al. 2003; Huffman et al. 2009), is beyond the scope of this study.

This study uses the comparisons mentioned above as a basis for drawing conclusions about the dependence of lightning on convective variables. Knowing that climate models are at least capturing where precipitation occurs (i.e., the spatial correlation) and that timing and magnitude are better captured over land facilitates the explanation of discrepancies that arise after the parameterizations are discussed below.

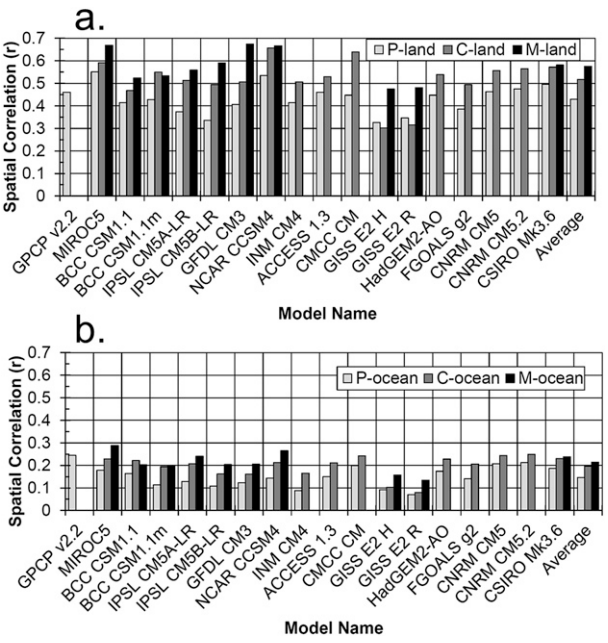

FIG. 2. Spatial correlation coefficient between observed lightning flash rate density from OTD/LIS, observed precipitation from GPCP, and precipitation, convective precipitation, and convective mass fluxes simulated by CMIP5 climate models used in this study. Comparisons are presented for (a) land and (b) ocean grid cells. High spatial correlation coefficients indicate that the location of lightning and the corresponding comparison fields are similar.

c. *Comparisons with lightning observations*

To make the case that climate model output convective parameters could be used to establish a relationship to deduce lightning flash rates, a simple linear model is derived for lightning as a function of total precipitation, convective precipitation, and convective mass flux. These results show that lightning is, to varying degrees, linearly correlated with modeled convective parameters, but that the linear model is also limited. Thus, a more complex empirical model is needed to better capture the variability. Furthermore, GPCP is used to show that the general relationship between total precipitation and lightning are similar for climate models. Figure 2 shows the linear correlation coefficients between mean monthly total precipitation (P), convective precipitation (C), and convective mass flux (M) with mean monthly lightning flash rate distributions (L) from OTD/LIS (Cecil et al. 2014) over land and ocean, where P-land, C-land, and M-land are the convective parameters over land, and P-ocean, C-ocean, and M-ocean are the values over ocean.

A comparison of P from GPCP versus L from OTD/LIS and P from the climate models versus L from OTD/LIS serves as a benchmark for how realistically the climate models capture broad-scale precipitation physics.

From Fig. 2, *P*-land and *P*-ocean from GPCP are significantly correlated with lightning (at greater than 95% confidence), but while the linear relationship explains 21% of the variance for land, the same relationship explains only 6% of the variance in the ocean-based data. Climate model *P*-land and *P*-ocean correlations with *L* are consistent with GPCP, with 18% of variance explained over land and 2% over oceans. Thus, *P* is generally not linearly related to *L*, but GPCP and climate models correlations are similar. This at least suggests that climate models capture broad-scale precipitation physics.

The expectation is that linear models using *C* and *M* would offer greater explanatory power. At local- and storm-level scales, *C* and *L* are related (Petersen and Rutledge 1998), so it is reasonable to expect that if model physics correctly capture large-scale patterns that emerge from microphysical processes, the correlation would generally increase for both the land- and ocean-based comparisons.

Figure 2 shows that, with the exception of NASA GISS-E2-R and GISS-E2-H over land, linear correlation of *C* with *L* is greater than that of *P* with *L*. Furthermore, the linear correlation of *M* with *L*, for the 10 climate models that archived *M* at CMIP5, also offers higher explanatory power than the correlation of *P* with *L* over land and ocean. The only exception to this is the BCC_CSM1.1(m) climate model.

Overall, the results in Fig. 2 offer some confidence that even with all the limits of climate models (poor spatial and temporal resolution compared with thunderstorm time and space scales, parameterization of physical processes that are key to lightning formation, etc.), the simulated physics of the climate models behave in a way that is consistent with observations from GPCP and from the general mechanism for lightning formation (Blyth et al. 2001; Deierling et al. 2005; Petersen and Rutledge 1998; Petersen et al. 2005). Namely, it appears that *C* and *M* are better predictors of *L* than *P*. Furthermore, climate models and GPCP show that while *P* is not a good predictor for *L*, they are similarly inaccurate.

However, the linear model captures less than half of the variance of *L* for both *C* and *M* (square of the correlation coefficients in Fig. 2). The climate model average linear correlation coefficients of *C*-land and *M*-land with *L*-land are 0.52 and 0.58, respectively. These values translate to 27% and 33% of variance in *L*-land captured, respectively. The analogous values for *C*-ocean and *M*-ocean are 4% and 5%, respectively. Thus, while linear correlation increases for the more convectively oriented model output, the variance explained by a linear model is not sufficient for accurate parameterization. A more complex empirical model is discussed in the next section.

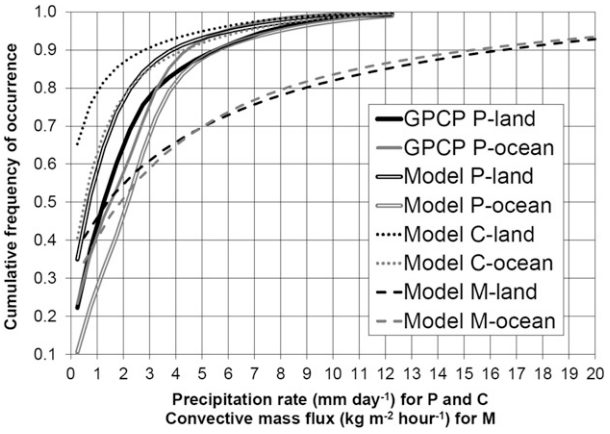

FIG. 3. Average cumulative frequency of occurrence for values of *P*-land, *P*-ocean, *C*-land, *C*-ocean, *M*-land, and *M*-ocean from the climate models, and *P*-land and *P*-ocean from GPCP.

3. Results

a. Lightning and convective parameters

Given the results shown in Figs. 1 and 2, this study first presents the discussion of the relationship between land-based mean monthly maps of lightning flash rate density from OTD/LIS (*L*-land) and land-based mean monthly maps of total precipitation (*P*-land), convective precipitation (*C*-land), and convective mass flux at the 0.44 hybrid-sigma pressure level (*M*-land). The relationship between ocean-based lightning (*L*-ocean) and convective parameters (*P*-ocean, *C*-ocean, *M*-ocean) is much weaker (Fig. 2b), but about 80% of lightning occurs over land (Allen and Pickering 2002; Cecil et al. 2014). Regardless of the lower accuracy over oceans, the globally complete results are presented below as well.

P-land, *C*-land, and *M*-land are binned, and the mean and a range of statistical percentiles (5th, 25th, 50th, 75th, 95th) of *L*-land in those bins are calculated. Binning is necessary to account for the heavily weighted frequency of occurrence of small values of all precipitation types, and to a lesser degree, values of *M*-land and *M*-ocean (Fig. 3). Figure 3 shows that ~90% of *P*-land from GPCP are less than 5.5 mm day^{-1}, and consistent with the low *P*-land climate model bias (Fig. 1b), ~90% of *P*-land from models are less than 4 mm day^{-1}. For *C*-land, ~90% of the simulated values are less than 3 mm day^{-1}, and ~65% of *C*-land are less than 0.25 mm day^{-1}. The *M*-land values are more evenly distributed than *P*-land and *C*-land, but they are still heavily biased (in terms of frequency of occurrence) to small values (Fig. 3). About 90% of *M*-land values are less than 16.5 kg m^{-2} h^{-1}, while 50% of *M*-land values are less than 1.5 kg m^{-2} h^{-1}. Thus, the mean and range of percentiles of values of *L*-land in each bin are calculated

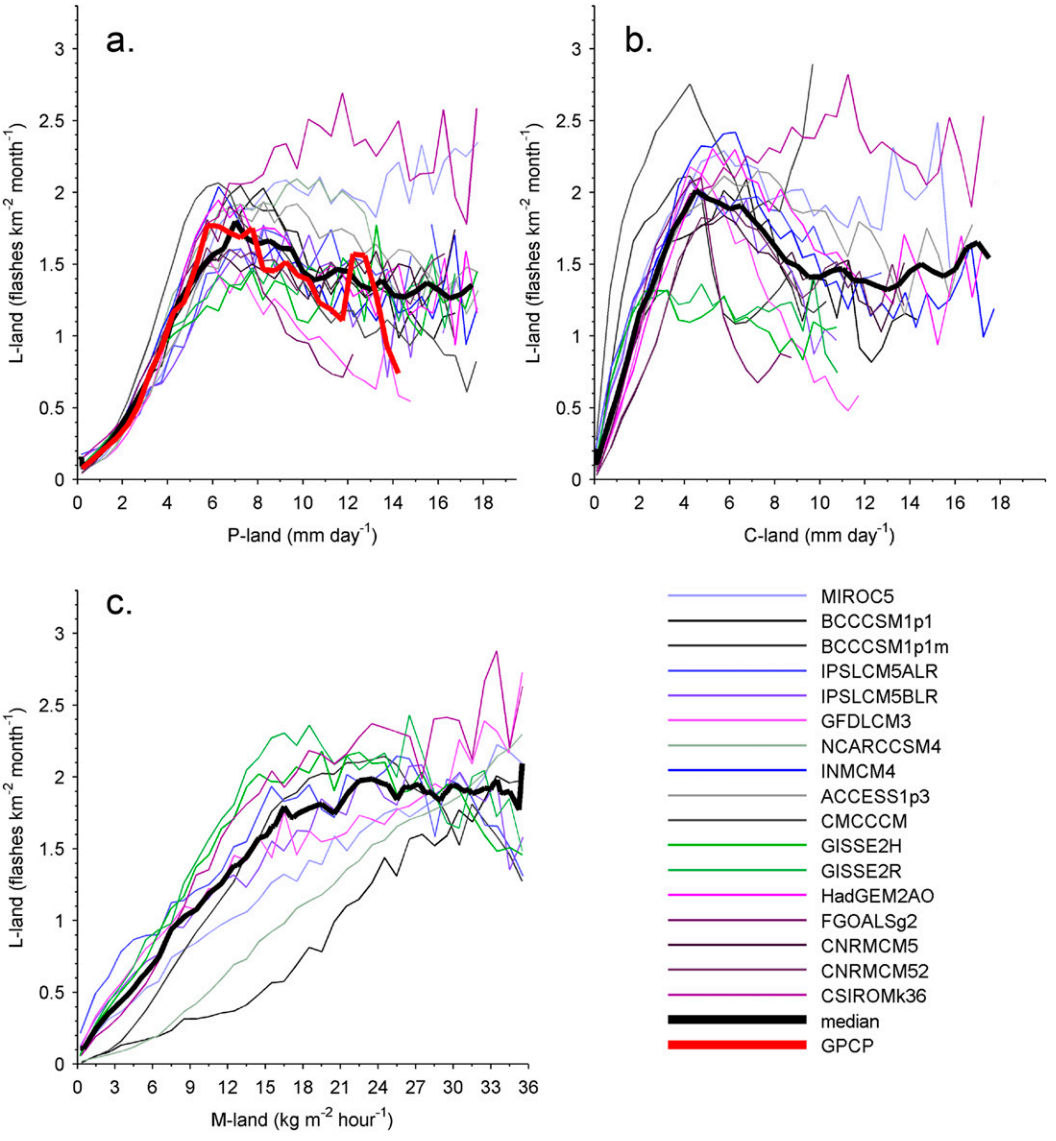

FIG. 4. The mean relationship between mean monthly *L*-land (flashes per square kilometer per month) and binned precipitation for (a) *P*-land (mm day^{-1}), (b) *C*-land (mm day^{-1}), and (c) *M*-land (kg m^{-2} h^{-1}). The multimodel median line (thick black line) is based on the values from the individual climate models listed in the legend. The mean value from the GPCP observationally based *P*-land dataset (thick red line) is also shown.

to understand the variability in *L*-land in each bin. Identical analyses are done for *L*-ocean with *P*-ocean, *C*-ocean, and *M*-ocean.

The analysis based on the mean values of *L*-land in each bin is shown in Fig. 4 for each climate model (various thinner lines) and for the median of all the climate model values (thick black lines). GPCP is shown (red) in Fig. 4a for the *L*-land dependence on *P*-land. The average agreement between GPCP and the multimodel median is ~10%, which is calculated as the mean percent difference of the thick black line from the thick red line in Fig. 4a. Climate models in general begin to diverge at 6–7 mm day^{-1}, but over 90% of *P*-land values are less than 6 mm day^{-1} (Fig. 3). Thus, to first order, the relationship of *L*-land and *P*-land is independent of whether *P*-land is from observations or climate models at the monthly time scale. The agreement with GPCP lends support to the idea that climate models are realistically capturing precipitation physics and that relationships between *L* and other convective parameters could be interpreted as realistic as well.

Figure 4b shows how *L*-land and *C*-land are related. The multimodel median value is shown again as a heavy black line. Several climate models (CMCC-CM, GISS-E2-H,

GISS-E2-R, and for larger values of *C*-land, GFDL CM3) diverge quickly from the multimodel median but the statistical median is not sensitive to outliers. Also, NCAR CCSM4 values of *C*-land were, on average, three orders of magnitude less than those reported by any other model (Table 1), so this climate model was excluded entirely from Fig. 4b. Overall, climate models tend to capture the physical connection between convection and lightning, as is evidenced by the abrupt rise in *L*-land as *C*-land increases from 0 mm day^{-1}.

Models tend to behave similarly for *C*-land $< 5\,\text{mm day}^{-1}$ (accounting for about 94% of cases) and then diverge for larger values (the remaining 6%). *L*-land increases approximately linearly for *C*-land $< 5\,\text{mm day}^{-1}$ and then decreases by about 25% for *C*-land between 5 and 10 mm day^{-1}. *L*-land remains relatively constant at ~1.5 flashes per square kilometer per month for larger ($>10\,\text{mm day}^{-1}$) monthly *C*-land values, which is similar to the behavior of *L*-land versus *P*-land (Fig. 4a).

Figure 4c shows how *L*-land and *M*-land are related. The relationship is, as the results of the linear model test in section 2c suggest, more linear than those shown in Figs. 4a,b. Fewer climate models contribute to the multimodel median value, but only the BCC CSM 1.1, BCC CSM 1.1m, and NCAR CCSM4 seem to exhibit different behavior of *L*-land for *M*-land $< 6\,\text{kg m}^{-2}\,\text{h}^{-1}$, which account for about 75% of the simulated values of *M*-land (Fig. 3). For *M*-land $> 21\,\text{kg m}^{-2}\,\text{h}^{-1}$, *L*-land is roughly constant at ~2 flashes per square kilometer per month.

The relatively constant (or decreasing) *L*-land at larger values of the mean monthly values of *P*-land and *C*-land in Figs. 4a,b is a feature of the model median curves, and to a lesser degree the model median curve for *M*-land. The GPCP relationship with *L*-land (Fig. 4a) is nearly the same as the climate model *P*-land relationship with *L* and provides observational support that this feature is not an artifact of the climate models. For reasons that are unclear, and perhaps better treated by a dedicated study, there seems to be a ''threshold'' of precipitation or convective precipitation beyond which lightning flash rate density remains constant. Convective mass flux seems less prone to this threshold effect, although the model median curve (Fig. 4c) does suggest nearly constant *L*-land beyond about 21 kg m^{-2} h^{-1}. For individual climate models in Fig. 4c, there are some climate models that exhibit a threshold effect [NASA GISS models, IPSL models, BCC_CSM1.1(m)], while other models do not exhibit a tapering-off effect at high values of *M*-land (CSIRO, GFDL, NCAR, BCC_CSM1.1, MIROC5). Field studies may be able to substantiate whether a physical basis for this threshold effect exists. In all cases, the high values of *P*-land, *C*-land, and *M*-land that suggest a threshold effect account for only a small subset (<10%) of the total number of occurrences (Fig. 3).

b. *Sensitivity of lightning dependence on convective parameters*

The statistical ranges of *L*-land for each of the bins (section 3a) of *P*-land, *C*-land, and *M*-land are shown in Fig. 5, and the range of *L*-land in each case represents the sensitivity of *L*-land to the particular value of *P*-land, *C*-land, and *M*-land. For example, the multimodel median curves for the interquartile range (25th–75th percentiles) in Fig. 5a suggest that at *P*-land = 5 mm day^{-1}, 50% of *L*-land values are between 0.12 and 2.1 flashes per square kilometer per month, with a mean value of 1.4 flashes per square kilometer per month. In Fig. 5b, when *C*-land = 5 mm day^{-1}, 50% of *L*-land values are between 0.62 and 2.8 flashes per square kilometer per month, with a mean value of 2.0 flashes per square kilometer per month. Similar ranges can be deduced in Fig. 5c for *L*-land versus *M*-land.

The ranges in Fig. 5 can generally be interpreted as uncertainty. At any particular value of *M*-land (Fig. 5c), for example, the results suggest that there is a wide range of *L*-land values that occurs based on the OTD/LIS dataset. The reason for this variability is unclear, but it likely results from the correspondingly wide range of microphysical to macrophysical processes necessary to produce lightning beyond simply the presence of convective precipitation or sufficient mass flux (Blyth et al. 2001; Deierling et al. 2005; Petersen and Rutledge 1998; Petersen et al. 2005; Williams 2005). Regardless, the variability in Fig. 5 helps to define the limits of interpreting the results of this study. In the end, the mean values shown in Fig. 4 and the thicker black lines in Fig. 5 by definition will tend to reproduce the mean lightning maps better than the extremes that may occur from one month to the next. Understanding the driving factors in the extremes in lightning flash rates—at monthly time scales—requires a study at finer time and space scales, which is beyond the scope of this study.

c. *Lightning over the oceans*

Figure 6 shows the mean *L*-ocean dependence on climate model convective parameters. The model median curve of *L*-ocean versus *P*-ocean (Fig. 6a) agrees to within ~50% compared to the corresponding curve using GPCP. This same comparison for *L*-land versus *P*-land (section 3a) results in ~10% difference (Fig. 5a). The poorer agreement in Fig. 6a is consistent with Fig. 1 discrepancies and is mainly due to large percentage errors at *P*-ocean $< 3\,\text{mm day}^{-1}$. Remarkably, there is very little model divergence at *P*-ocean $< 3\,\text{mm day}^{-1}$ in spite of the poorer skill in models capturing ocean precipitation.

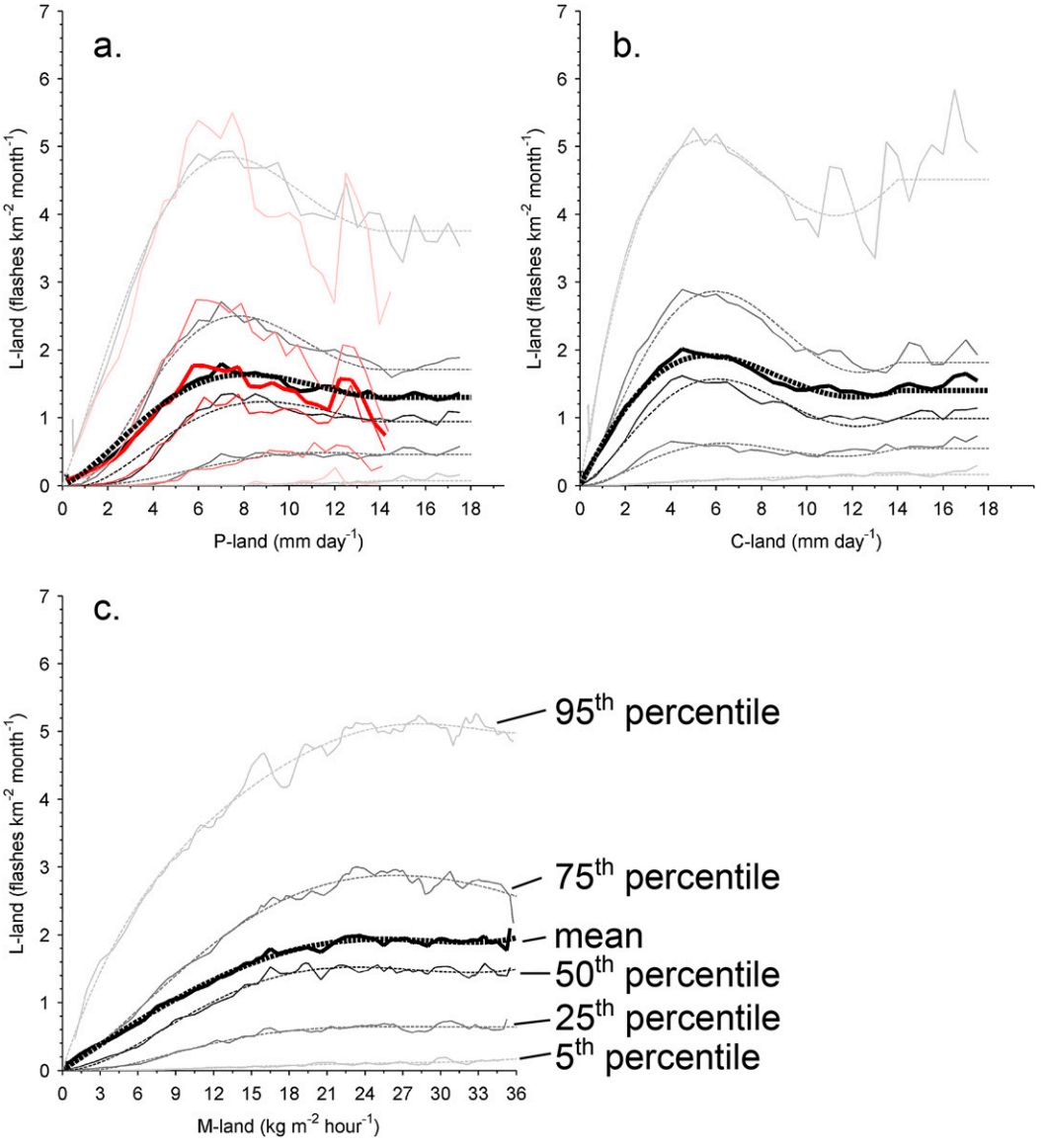

FIG. 5. The mean and statistical percentiles of the range of values of L-land (flashes per square kilometer per month) for each value of (a) P-land (mm day^{-1}), (b) C-land (mm day^{-1}), and (c) M-land (kg m^{-2} h^{-1}). The multimodel median is shown in shades of black, GPCP is the dark gray solid line near the mean values curve in (a). The polynomial parameterizations [e.g., (1), Table 2] for each percentile are overlaid as dashed lines.

Model median L-ocean remains relatively constant at ~0.1 flashes per square kilometer per month for P-ocean > 6 mm day^{-1} (Fig. 6a). For L-ocean versus C-ocean (Fig. 6b), L-ocean converges on ~0.1 flashes per square kilometer per month for C-ocean > 3 mm day^{-1}. Figure 6c shows the relationship between L-ocean and M-ocean. In this case, L-ocean linearly increases for M-ocean < 15 kg m^{-2} h^{-1} before linearly decreasing and then remaining relatively constant. In all cases, L-ocean values remain roughly an order of magnitude less than L-land values (Fig. 4) for equivalent bins of P, C, and M even though the cumulative frequency of occurrence is generally similar for ocean and land (Fig. 3), especially for M-land and M-ocean.

d. *Robust linearity in lightning dependence on convective parameters*

There is evidence of a robust linear feature in the dependence of lightning on the different convective parameters. In Figs. 4b, 5b, L-land increases linearly with increases in C-land for values of C-land less than 4–5 mm day^{-1} (Fig. 5b). This linear behavior is more evident for M-land (Fig. 5c) for values less than 15 kg m^{-2} h^{-1}. Figure 4 shows that most climate models seem to exhibit

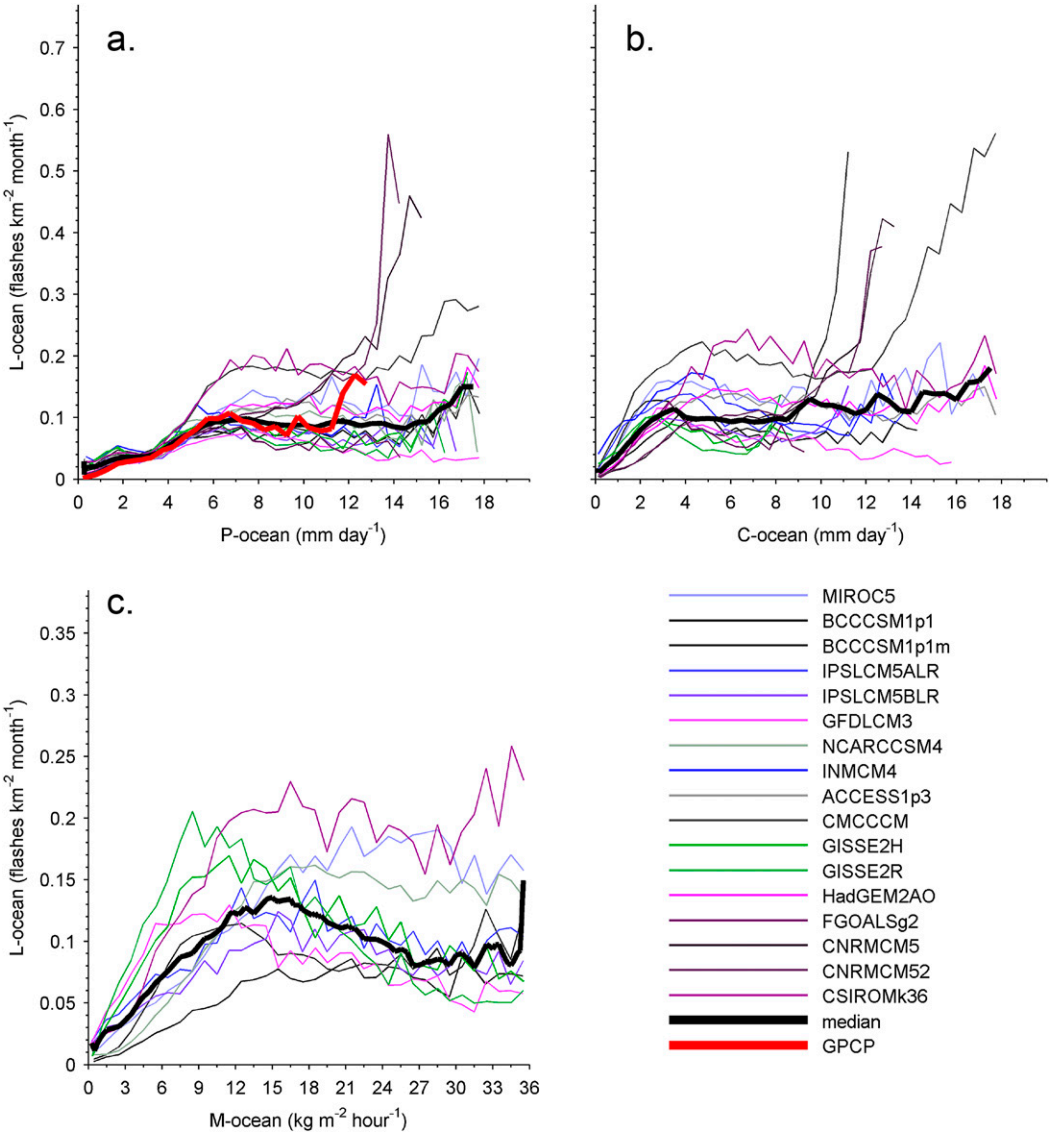

FIG. 6. The mean relationship between mean monthly *L*-ocean (flashes per square kilometer per month) and binned precipitation for (a) *P*-ocean (mm day^{-1}), (b) *C*-ocean (mm day^{-1}), and (c) *M*-ocean (kg m^{-2} h^{-1}). The multimodel median line (thick black line) is based on the values from the individual climate models listed in the legend. The mean value from the GPCP observationally based *P*-ocean dataset (thick red line) is also shown.

this linearity but to varying degrees depending on the model.

This linearity could be an important feature, since Fig. 3 shows that ~90% of the climate model convective precipitation values (*C*-land, *C*-ocean) are less than ~5 mm day^{-1}, and ~90% of climate model convective mass flux values (*M*-land, *M*-ocean) are less than ~15 kg m^{-2} h^{-1}. A major component of the mean monthly, coarse grid-scale lightning can then be captured by this linear dependence of lightning on simulations of convective parameters. Nonlinearity in the dependence of lightning on convective parameters arises for the largest, and least frequently occurring, values of *C*-land, *C*-ocean, *M*-land, and *M*-ocean.

The variance explained by a linear model of *L*-land using *C*-land from 0 to 5 mm day^{-1} averages 86% across the range of statistical percentiles (Fig. 5b). The variance explained by a linear model of *L*-land using *M*-land from 0 to 15 kg m^{-2} h^{-1} averages 89% (Fig. 5b). For *L*-ocean, the variance explained by *L*-land relationships with *C*-land and *M*-land is 72% and 80%, respectively. Compared to the results discussed in section 2c, which suggested a linear model is not generally sufficient, the linearity discussed here suggests that for a limited range

of frequently occurring values of convective precipitation and convective mass flux from the climate models, a linear model is quite applicable. The nonlinear dependence of lightning on convective parameters is discussed in the next section.

e. *Empirical lightning parameterization*

Since the linear models (sections 2c and 3d) are limited in their explanatory power, a more complex model is used to establish a more generally applicable empirical fit to the climate model relationships with OTD/LIS data. Theoretical and field studies of thunderstorms have shown that lightning flash rates are proportional to the product of downward flux of solid precipitation (graupel) and upward flux of ice crystals into the anvil of a storm (e.g., Blyth et al. 2001; Deierling et al. 2008). The linear models (sections 2c and 3d) suggest that climate models capture this fundamental relationship to some degree with the less precise measures of convection via C and M, but the spatial and temporal scales in this study require empirical analysis for the most general application. Namely, climate model spatial resolution does not resolve individual clouds, let alone individual thunderclouds.

Although there is no theoretical basis, an empirical polynomial fit to the relationship between L and both C and M has been discussed previously in the context of ground-based lightning data from the U.S. National Lightning Detection Network (Orville et al. 2011) and a high-temporal-resolution (~6 hourly output) general circulation model output (Allen and Pickering 2002). This study tests multiple polynomial fits to the relationship between global satellite-based lightning data from OTD/LIS and global climate model output.

Polynomial functions ranging from first to ninth degree were tested as fits to the thick black lines shown in Figs. 4–6. To select a specific polynomial fit, the root-mean-square (RMS) difference is calculated as the difference between the multimodel median curve (e.g., solid lines in Fig. 5) and the fit curve (e.g., dashed lines in Fig. 5). Figure 7a shows this RMS difference as a function of polynomial degree for C-land and M-land, and the average of the two curves as a black line. Figure 7b shows the percent improvement in the RMS difference as a function of polynomial degree, calculated as the change in RMS difference compared to the previous value. In both cases, the values for first- and second-degree polynomial fits are intentionally not shown since, except for M-land, the values are too large.

Overall, the average fit to the multimodel median curve improves as the polynomial degree increases from first to fourth degree, and more modestly from fourth- to fifth-degree polynomial. Further improvements beyond a fifth-degree polynomial were less than 10% on average.

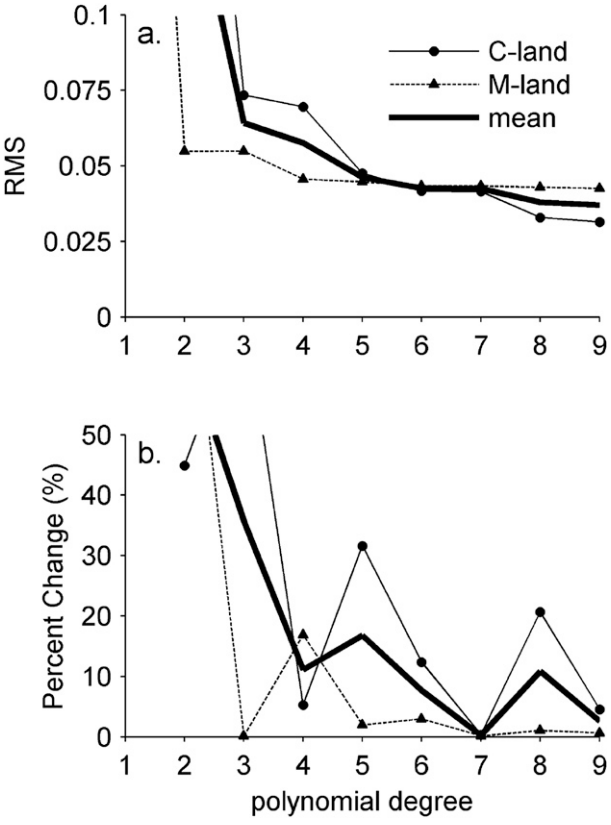

FIG. 7. The (a) RMS difference between the multimodel median curve and empirical polynomial fit as a function of increasing polynomial degree, and (b) percent change in the RMS difference calculated as the RMS difference at a specific polynomial degree compared to the RMS difference from the previous polynomial degree.

Polynomial fits greater than fifth degree are more likely to fit the noise in the model median curves rather than the overall signal. A fourth-degree polynomial fit has been used previously (Allen and Pickering 2002), but because statistical improvements were evident for a more complex fifth-degree polynomial (especially for C-land, Fig. 7b), the focus in this study is on a fifth-degree polynomial fit. The choice is somewhat subjective, and strives to use a single-polynomial fit that balances RMS improvements and model complexity.

The functional form used in this study to understand how L and convective parameters are related is

$$L = a_1X + a_2X^2 + a_3X^3 + a_4X^4 + a_5X^5, \qquad (1)$$

where L is the monthly lightning flash rate density (flashes per square kilometer per month) and X is one of either P (mm day^{-1}), C (mm day^{-1}), or M (kg m^{-2} h^{-1}) for land or ocean grid cells, and a_1–a_5 are the fit coefficients (Table 2). The curves from (1) using a relevant

TABLE 2. Fit coefficients for the empirical model ($L = a_1X + a_2X^2 + a_3X^3 + a_4X^4 + a_5X^5$; see text) for mean lightning flash rate density that occurs as a function of P, C, or M over land (P-land, C-land, M-land) and ocean (P-ocean, C-ocean, M-ocean). Replace X in the equation with P-land, C-land, M-land, or P-ocean, C-ocean, M-ocean, where precipitation rates (mm day^{-1}) are the monthly averaged values, while convective mass flux (kg m^{-2} h^{-1}) is the monthly value through the 0.44 hybrid-sigma pressure level. The output is monthly lightning flash rate density (flashes per square kilometer per month).

Input variable	a_1	a_2	a_3	a_4	a_5
P-land (mm day^{-1})	1.43×10^{-1}	8.01×10^{-2}	-1.52×10^{-2}	9.11×10^{-4}	-1.82×10^{-5}
C-land (mm day^{-1})	6.54×10^{-1}	-2.86×10^{-2}	-9.63×10^{-3}	1.01×10^{-3}	-2.69×10^{-5}
M-land (kg m^{-2} h^{-1})	1.31×10^{-1}	-1.93×10^{-3}	8.87×10^{-5}	-6.84×10^{-6}	1.17×10^{-7}
P-ocean (mm day^{-1})	3.26×10^{-2}	-7.16×10^{-3}	1.02×10^{-3}	-7.31×10^{-5}	1.93×10^{-6}
C-ocean (mm day^{-1})	5.11×10^{-2}	-1.04×10^{-2}	1.09×10^{-3}	-5.66×10^{-5}	1.17×10^{-6}
M-ocean (kg m^{-2} h^{-1})	1.06×10^{-2}	6.71×10^{-4}	-8.58×10^{-5}	2.41×10^{-6}	-1.97×10^{-8}

coefficient from Table 2 are shown in Fig. 5 for the land-based component of the study. Ocean-based results are similar; coefficients for those fits are in Table 2. As a physically based constraint, the constant term in the polynomial is set to zero such that when P, C, or M is zero, then L is zero. The high-degree polynomial function is extremely flexible, but for P and C, the fit is limited to an upper limit of 14 mm day^{-1}, as is evident in Figs. 5a,b. The upper limit is chosen from the GPCP data, which suggest that 99.6% of observed monthly total precipitation is less than 14 mm day^{-1}. The full range of M is used in the empirical fit (0–36 kg m^{-2} h^{-1}).

f. Evaluation of the empirical lightning parameterization

To evaluate the parameterization, L-land and L-ocean are calculated using the values in Table 2 and (1), and the complete (land–ocean) map of lightning flash rate density derived from the parameterization is first compared against observed lightning from OTD/LIS. To harmonize the comparisons and to facilitate a multimodel median set of convective parameters (P, C, M), the monthly climate model output fields are interpolated to a common 2° × 2.5° latitude–longitude grid (i.e., GFDL CM3 from Table 1) for this analysis. Total lightning flash rate density is then from the combination of L-land and L-ocean determined by Table 2 and (1).

Mean annual L from OTD/LIS and L from the parameterizations using C and M (Table 2) are shown in Figs. 8a–c, using a logarithmic scale for lightning flash rate density. Values of L derived from P are not shown—P is a poor predictor of L as discussed above—and values of L from C and M are both shown, since not every climate model includes M as output (Table 1). Statistics at the top of the mean annual lightning maps (Figs. 8a–c) are the mean annual flash rates for the globe, land, and ocean (in units of flashes per second), and the spatial correlation coefficient (r) for globe, land, and ocean (Figs. 8b–c compared against Fig. 8a).

Mean annual L from OTD/LIS is well captured. The global flash rate from OTD/LIS is 47 flashes per second (consistent with Cecil et al. 2014), while the parameterizations using C and M produce a global mean annual flash rate of 50 and 44 flashes second, respectively. Land and ocean mean annual flash rates are also similar to OTD/LIS.

The parameterization underestimates lightning off the eastern coasts in the Northern and Southern Hemisphere midlatitudes and off the western coasts in the deep tropics, while overestimating lightning in much of the open ocean (Fig. 8). Outside of the intertropical convergence zone (ITCZ), the spatial patterns over the oceans are captured by the parameterization. The discrepancies in magnitude may be driven by coastal dynamics that are poorly captured by coarse-resolution global climate models such as sea- and land-breeze circulations and frontal passages. To address this discrepancy, vertically resolved ice mass (Blyth et al. 2001; Deierling et al. 2008), which is unavailable from the CMIP5 archives, could be useful, especially in the ITCZ. A functional dependence on land–ocean thermal contrasts (Williams and Stanfill 2002) may also be an interesting way to improve the ocean-based parameterization.

Over land, mean annual lightning flash rate density is underestimated over Argentina, much of Africa, the southern United States, Central America, and northern India (Fig. 8). This underestimation is likely related to the coarse time resolution of the data in this study compared to the high fraction of annual lightning that occurs in the relatively less frequent large thunderstorms (Cecil et al. 2005; Zipser et al. 2006). Land surfaces in the northern latitudes such as Northern Europe, northern North America, and northern Russia are better captured by the parameterization using M than C. Mean annual lightning over the United States is also better captured by the parameterization using M than C.

Figures 8d,e show the spatially explicit temporal correlation coefficients for each grid box. This is a calculation of the 12-month temporal correlation between OTD/LIS

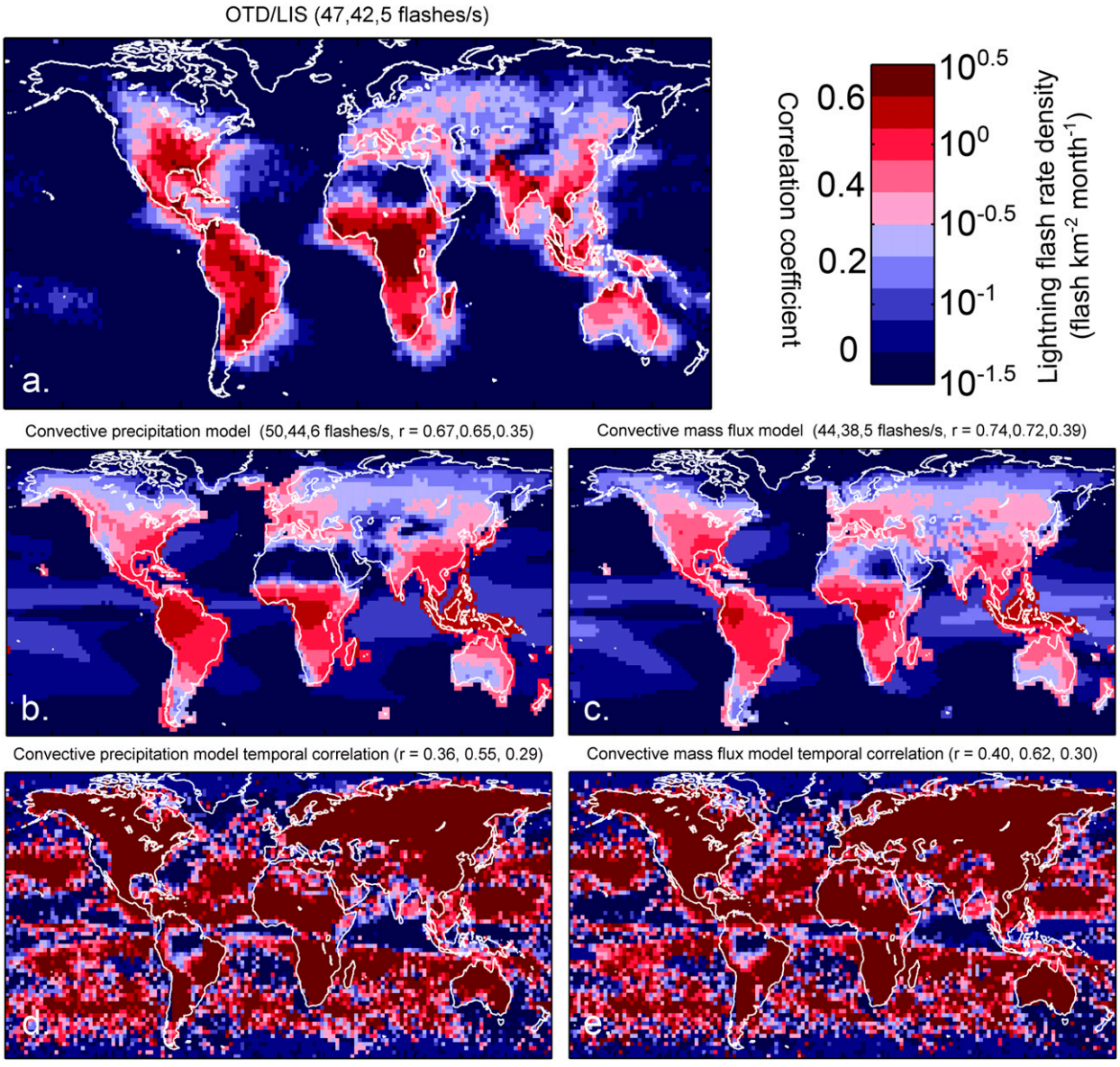

FIG. 8. Maps of mean annual lightning flash density (flashes per square kilometer per month) from (a) OTD/LIS, (b) the parameterization based on *C*-land and *C*-ocean, and (c) the parameterization based on *M*-land and *M*-ocean. Also shown are maps of seasonal correlation coefficients between OTD/LIS mean monthly lightning and (d) parameterized lightning based on *C*-land and *C*-ocean and (e) parameterized lightning based on *M*-land and *M*-ocean. Statistics at the top of the lightning maps (a)–(c) are the mean annual flash rates for the globe, land, and ocean (flashes per second), and the spatial correlation coefficient for globe, land, and ocean between OTD/LIS and the derived lightning maps is shown in (b) and (c). The statistics at the top of (d) and (e) are the spatially averaged mean seasonal correlation coefficients for the globe, land, and ocean.

mean monthly lightning and lightning derived from *C* and *M*. The statistics at the top of Figs. 8d,e are the spatially averaged temporal correlation coefficients for globe, land, and ocean, respectively.

The parameterization based on *C* captures seasonality in *L* (temporal correlation) with better than 95% confidence in 63% of land and 32% of ocean surfaces (Fig. 8d), while Fig. 8e shows that seasonality in *L* is captured with 95% confidence by the *M*-based parameterization for 69% of land and 30% of ocean surfaces. The seasonality of ocean-based lightning is poorly captured by the parameterization, but the temporal distribution of land-based lightning is well captured.

A final note about the results is that limiting the analysis of the dependence of *L* on *C* to the 10 climate models that output both *C* and *M* (Table 1) does not

change any of the results. The spatiotemporal correlation coefficients and mean annual lightning flash rates are nearly identical to those shown in Fig. 8 and discussed above.

4. Discussion

Over land surfaces, the parameterization tends to underpredict L in areas with the most lightning, such as the tropics, and to overpredict L in areas with the least lightning, such as northern boreal forests (Figs. 8a–c). These discrepancies could partly be attributed as an artifact of parameterizing global lightning against the mean monthly value of lightning as opposed to lightning that varies on an annual basis. A parameterization to the mean will tend to reproduce the mean as opposed to the low- and high-magnitude lightning flash rates. This idea is evident by using the statistical percentiles shown in Fig. 5. Although this is not shown, parameterization to each percentile of lightning produces nearly identical spatial and temporal correlation coefficients as those shown for the mean case in Fig. 8 (e.g., 0.74 spatial correlation in Fig. 8c, 0.62 temporal correlation for land-based lightning in Fig. 8e). The lightning flash rate density simply scales up and down relative to the mean. Thus, parameterization to high lightning flash rate density (say, 95th percentile) tends to produce higher lightning flash rate density without affecting the spatiotemporal patterns. The same is true for other percentiles. An improved parameterization would then result from focusing on a method to increase the spatiotemporal correlation.

One method to improve spatial and temporal correlation is to derive a parameterization using a lightning time series as opposed to a mean monthly climatology. Although LIS is not global, Cecil et al. (2014) discuss the interannual variability in monthly lightning flash rates from the LIS time series and find that there is no significant trend over the last decade, and very little interannual variability. In a regional analysis of LIS data from the past decade, however, Albrecht et al. (2011) found that lightning trends were negative in the tropics and subtropics viewed by TRMM. Regardless, a complete global time series of lightning is not yet available for testing. North American Lightning Detection Network (NALDN; Orville et al. 2011), World Wide Lightning Location Network (WWLLN; Lay et al. 2004; Virts et al. 2013), or Global Lightning Dataset (GLD360) (Pohjola and Mäkelä 2013; Said et al. 2010, 2013) data could act as independent datasets for testing global climate model parameterization, but each dataset has limits. NALDN is limited mainly to cloud-to-ground lightning in Canada and the United States. WWLLN sensor coverage has only been adequate for global lightning detection since about 2008 (Abarca et al. 2010). GLD360 has only been in operation since about 2009.

Another method to improve the spatiotemporal correlations between derived and observed lightning is by increasing the complexity of the parameterization beyond simply P, C, or M. Convective regimes and land–ocean lightning biases are aspects that the parameterization oversimplifies. Shifting convective regimes in places like the Amazon (Williams et al. 2002) may become evident by evaluating the seasonal dependence of the coefficients of the parameterization. Vertically resolved ice mass flux, which is critical to the charging mechanism that produces lightning (Blyth et al. 2001), is unavailable from CMIP5 model output archives, but it may be less dependent on land–ocean biases than convective mass flux. Some CMIP5 climate models likely do save vertically resolved ice mass flux as model output for diagnostic purposes outside of the CMIP5 data portal.

The seasonality of lightning is best captured by parameterization using M (Fig. 8e), with the western United States, India, Australia, and Southeast Asia showing improvements compared to the parameterization using C (Fig. 8d). Seasonality is not well captured by either parameterization for much of the oceans. Over land, equatorial South America over the Amazon is poorly captured by both parameterizations, suggesting that climate models are not capturing the regional characteristics of convection there. The known maritime-like and land-like convective regimes of equatorial South America (Williams et al. 2002) could also motivate further study into the existence of regional or seasonal dependencies of the parameterization coefficients.

Regional discrepancies could also be due to inaccuracies in climate model simulations of precipitation (e.g., Meehl et al. 2012; Randall et al. 2007) that arise from subgrid-scale convective processes that are important in determining precipitation rates and difficult to accurately capture at the spatial scales involved in climate modeling. The complex hydrological cycle over the Amazon rain forest (Williams et al. 2002), the monsoon seasonality of India, coastal transition regions, and topographic flow regimes all are involved in determining the accuracy of global and regional precipitation simulated by climate models (e.g., Donner et al. 2011; Dufresne et al. 2013; Gent et al. 2011; Wu et al. 2010). For example, a coastal region like the western United States, where lightning plays an important role in spring and summertime fire activity, may be missing some of the topographic-driven convective precipitation that drives summer rains while at the same time overestimating the winter rains from Pacific cyclones. Both would act to

decrease the seasonal correlation and to increase uncertainty in the parameterization in that region.

Ocean-based lightning is often poorly simulated. This is likely due to the fact that seasonal ocean-based precipitation rates from climate models are poorly simulated when compared with GPCP (Fig. 1), and that the lightning frequency is also much smaller over oceans than land (Cecil et al. 2014; Pessi and Businger 2009). Discrepancies between simulated and observed maritime lightning downstream of land surfaces in the tropics and midlatitudes are one problem with the parameterization in this study. This touches on the large land–ocean ratio of lightning flashes (e.g., Allen and Pickering 2002; Cecil et al. 2014; Williams and Stanfill 2002). Namely, the choice for calling a model grid cell ''land'' or ''ocean'' (section 2a) could be relaxed further to allow ''near land'' grid cells to be considered land or to be parameterized independently of land and ocean. Allen and Pickering (2002) suggested this as a strategy to improve their parameterization, but they pointed out that this classification may be too arbitrary to be justified (i.e., overfitting).

The near-land maxima (east of the United States, southern Africa, South America, and Australia, and west of Central America) is also accompanied by near-land/coastal minima in lightning (west of many of those continents and countries). Thus, overclassification of land and ocean would result in a middle-ground parameterization. Allen and Pickering (2002) found that convective mass flux was a better predictor of lightning in those near-land locations, and the results of this study agree. For example, northwestern North America and southern Alaskan coastlines have a band of high lightning flash rate density when using C to parameterize lightning (Fig. 8b), but this high lightning band is muted when using M (Fig. 8c). Similarly, coastlines and maritime-like convective regimes (Williams and Stanfill 2002) such as Scandinavia, the British Isles, southwestern South America, and New Zealand are better captured using M to parameterize lightning. In all those examples, however, the parameterization still overestimates lightning.

Previous studies have discussed global lightning parameterizations (Allen and Pickering 2002; Price and Rind 1992; Tost et al. 2007). Allen and Pickering (2002) analyzed multiple schemes for parameterizing global lightning from general circulation model output that included convective precipitation (C), cloud-top height, and convective mass flux (M), and found that M captured global lightning most accurately, while cloud-top height was least accurate. Two important notes about Allen and Pickering (2002) are that they compared results against OTD from a single year (1996) and that their parameterizations were against cloud-to-ground lightning and, as such, had to be scaled using cloud-top height (Price and Rind 1993) to draw a comparison with total lightning from OTD. With those notes in mind, Fig. 9 displays global- and zonally averaged flash rates using zonal bands that are identical to those used by Allen and Pickering (2002), so that a direct comparison of results from this study with their results can be made.

The results in Figs. 8, 9 suggest that M is the most accurate way to parameterize global lightning on a monthly time scale. The accuracy of zonally averaged lightning flash rates is evaluated against OTD/LIS in Fig. 9. Average RMS differences from OTD/LIS are 20%–60% less for lightning derived from the parameterization with M than for C except for the zone from the equator to 20°N (Fig. 9d), where average RMS is 4.0 flashes per second for M and 3.8 flashes per second for C (about 5% larger). Temporal correlation with OTD/LIS improves for all cases except the global average (Fig. 9a) using the parameterization based on M. Figure 9 also shows that the results of this study are in broad agreement with those of Allen and Pickering (2002) in that M is the best metric for parameterizing lightning in climate or global-scale models. Unlike Allen and Pickering (2002), C is shown to be a reasonable second choice for determining lightning, which is useful if M is not available as output (Table 1). The improvement in deriving lightning from C since Allen and Pickering (2002) may be a result of general improvements in climate model precipitation physics over the past two decades (e.g., Donner et al. 2011; Dufresne et al. 2013; Gent et al. 2011; Randall et al. 2007; Wu et al. 2010).

The Southern Hemisphere tropics (Fig. 9c) has the poorest temporal correlation with OTD/LIS. Lightning derived from the parameterization lags lightning from OTD/LIS by one month in the zonal region and also, to a lesser degree in the Northern Hemisphere tropics (Fig. 9d). The lag in flash rates is largely driven by the land-based component of the parameterization, since ocean-based lightning, even in a region with a large fraction of surface area being ocean, contributes 5–10 times less lightning than land. Interestingly, Allen and Pickering (2002) used a different type of global model, but their results showed the same lag in the tropics (Fig. 9) when compared to OTD/LIS. Most likely, this lag is a result of the relatively poor ability of climate models to capture precipitation physics in the tropics, and in particular over the unique convective regimes (Williams et al. 2002) over equatorial South America. Figure 1b shows that temporal correlation of land-based precipitation with GPCP depends strongly on the model, which suggests some of the problems in climate model simulation of land-based tropical precipitation.

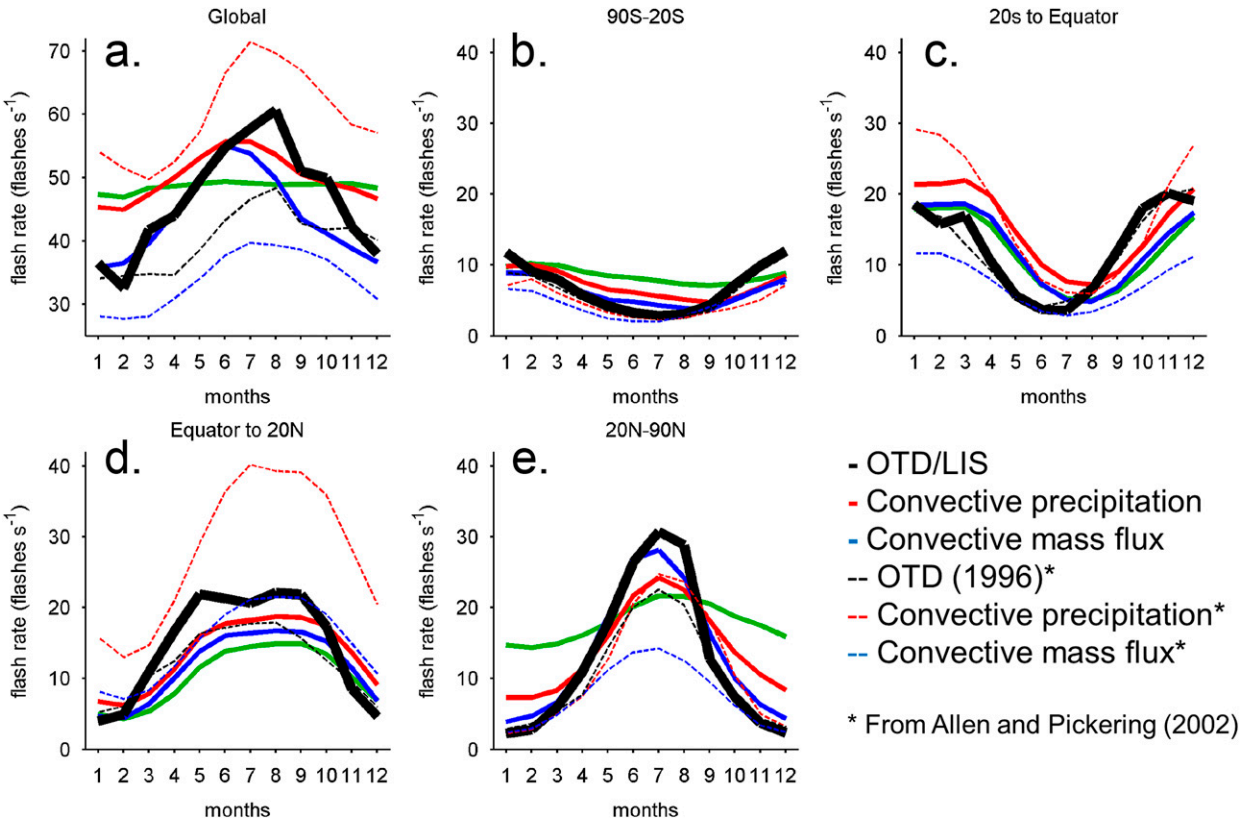

FIG. 9. Mean monthly total (land and ocean) lightning flash rates (flashes per second) from OTD/LIS (black line), the lightning parameterizations using *C*-land and *C*-ocean (red solid line) and *M*-land and *M*-ocean (blue solid line), and lightning parameterizations from Allen and Pickering (2002) using convective precipitation (red dashed line) and convective mass flux (blue dashed line). Also shown are the 1996 OTD lightning averages from Allen and Pickering (2002). The averages are shown for the (a) globe, (b) southern extratropics (90°–20°S), (c) southern tropics (20°S to the equator), (d) northern tropics (equator to 20°N), and (e) northern extratropics (20°–90°N).

An interesting and potentially important feature that emerges from the lightning parameterization is linearity over a subset of the full range of values of *C* and *M* from climate models. This linearity is prominent in Figs. 4–6, and is also apparent in the observationally based analysis of OTD/LIS compared with GPCP in Figs. 4a, 6a for total precipitation greater than $\sim 2\,\mathrm{mm\,day^{-1}}$. The observational basis suggests that the feature is not purely a climate model artifact, since OTD/LIS and GPCP are entirely independent of climate model simulations. This linearity suggests that lightning increases proportionally with *C* and with *M* for $C < 4$–$5\,\mathrm{mm\,day^{-1}}$ and $M < 15$–$16\,\mathrm{kg\,m^{-2}\,h^{-1}}$. As Fig. 3 shows, ~90% of *C* and *M* values simulated by the climate models are less than those upper limits to linearity.

The results in this study suggest lightning flash rate changes are proportional to changes in relatively small values of *C* and *M*. Climate models from the previous CMIP show that *M* is expected to decrease 10%–20% over the next century (Vecchi and Soden 2007), and observational evidence shows lightning trends from LIS are generally negative over the last decade (Albrecht et al. 2011). However, the climate model trends tend to reflect changes in *M* driven by the intense convection in the tropics (Vecchi and Soden 2007), while LIS is necessarily tropical. The linearity could then be a valuable way to assess how climate model projections of convection will impact future lightning distributions at both global and regional spatial scales.

5. Summary

This study examines whether convective parameters simulated using current CMIP5 climate models can be used to derive lightning. The physical basis for this parameterization emerges from theoretical, field, and higher-resolution modeling studies of thunderstorm dynamics that suggests that the mass flux of ice in the presence of supercooled water is related to lightning flash rate (Barthe et al. 2010; Blyth et al. 2001; Deierling et al. 2005). The approach in this study, however, uses mean monthly lightning and climate model output.

Although climate models are not able to resolve the time and space scales associated with a single thunderstorm, and are generally not intended to simulate day-to-day weather, the multiyear mean monthly convective parameters like convective precipitation and convective mass flux should, in principle, be related to the average lightning observations.

The OTD/LIS satellite-based global lightning data and output from 17 climate models (Table 1) are used to test the hypothesis that monthly convective parameters can be used to predict lightning. GPCP-observed global monthly precipitation data are also used to provide some observational evaluation of the climate model precipitation physics. A fifth-order polynomial function is used to capture the nonlinear relationship between monthly lightning and monthly convective parameters. The climate model convective parameters this study focuses on are convective precipitation and the upward convective mass flux at a pressure level of ~427 hPa (or near the hybrid-sigma pressure level of ~0.44).

Climate model convective mass flux is the best predictor of lightning, as determined by spatiotemporal correlation and magnitude comparisons with OTD/LIS. Overall, lightning derived from the convective mass flux parameterization captures about 55% of the spatial variability in mean annual lightning and global flash rates are within about 6% of OTD/LIS. The parameterization works better over land and tends to underpredict lightning over regions with the highest flash rates, while overpredicting lightning for regions with the lowest flash rates.

A feature of the relationship between monthly lightning and monthly convective parameters is linearity for the low values of convective precipitation and convective mass flux. Whereas a nonlinear function is needed to parameterize the full range of simulated convective precipitation and convective mass flux, a linear function captures 70%–90% of the OTD/LIS variability for a range of convective precipitation and convective mass flux values that account for ~90% of the total range. This linear characteristic of the relationship between lightning and climate model convective parameters is clear in Figs. 4b,c. If convective precipitation and convective mass flux change in the future as a result of the perturbations to the Earth system that are already underway (e.g., Christensen et al. 2007), then the linear dependence of lightning on those convective parameters should be considered.

The parameterization in this study is immediately relevant to communities of global climate modelers. Paleo, historical, and projection studies using climate models can all take advantage of the results to create simulated lightning maps for studies of the time history of lightning distributions and at least relative changes in magnitude. Global fire modeling is physically confined to land but logistically confined to the mean monthly climatology from OTD/LIS. Hence, this parameterization would likely be a way to test how variability in lightning affects global fire distributions over long time scales (Kloster et al. 2010; Li et al. 2012; Pechony and Shindell 2009; Thonicke et al. 2010). Considering that global chemical modeling is a prominent reason for the development of lightning parameterizations (e.g., Allen and Pickering 2002; Price and Rind 1992; Price et al. 1997; Tost et al. 2007), the results in this study are highly relevant in determining monthly lightning contributions to the nitrogen cycle.

The methods in this study are readily adaptable to changes in climate model output, specific climate model or global model experiments, or changes to the availability or quality of lightning data. As climate models improve simulation of microphysical and precipitation processes (Lebsock et al. 2013), the parameterization in this study can be revisited. Global climate models are used in this analysis, but output from a wider range in models (such as cloud-resolving models, regional climate models, or Earth system models) could be used as a basis for the parameterization. The OTD/LIS dataset continues to develop in size and quality (e.g., Cecil et al. 2014) and may be used to further test the robustness of the parameterizations. Additional satellite-based (Liu et al. 2011) or ground-based (Orville et al. 2011) datasets could also supplement the OTD/LIS dataset, especially at high latitudes where coverage is limited to the OTD observational period. Thus, improvements or changes in any aspect of the observational or simulations can be incorporated to produce a new statistical parameterization using methods discussed in this study.

Acknowledgments. Thanks go to CMIP and the climate modeling groups (Table 1) for making their model output available. For CMIP, the U.S. Department of Energy's PCMDI provided coordinating support and led development of software infrastructure in partnership with the Global Organization for Earth System Science Portals. Thanks also go to scientists maintaining and distributing GPCP and OTD/LIS datasets, to three reviewers for taking the time to provide very useful and constructive feedback through peer-review, and to Paul Ginoux and Matt Eastin for comments on an early draft. Funding supporting this research was from UNC Charlotte Geography and Earth Sciences Department, NC Space Grant, and NSF BCS-14364961436496.

REFERENCES

Abarca, S. F., K. L. Corbosiero, and T. J. Galarneau, 2010: An evaluation of the Worldwide Lightning Location Network (WWLLN) using the National Lightning Detection Network (NLDN) as ground truth. *J. Geophys. Res.,* **115,** D18206, doi:10.1029/2009JD013411.

Adler, R. F., and Coauthors, 2003: The Version-2 Global Precipitation Climatology Project (GPCP) monthly precipitation analysis (1979–present). *J. Hydrometeor.,* **4,** 1147–1167, doi:10.1175/1525-7541(2003)004<1147:TVGPCP>2.0.CO;2.

Albrecht, R. I., S. J. Goodman, W. A. Petersen, D. E. Buechler, E. C. Bruning, R. J. Blakeslee, and H. J. Christian, 2011: The 13 years of TRMM Lightning Imaging Sensor: From individual flash characteristics to decadal tendencies. *Proc. XIV Int. Conf. on Atmospheric Electricity,* Rio de Janeiro, Brazil, International Commission of Atmospheric Electricity, 4 pp. [Available online at http://ntrs.nasa.gov/archive/nasa/casi.ntrs.nasa.gov/20110015779.pdf.]

Allen, D. J., and K. E. Pickering, 2002: Evaluation of lightning flash rate parameterizations for use in a global chemical transport model. *J. Geophys. Res.,* **107,** 4711, doi:10.1029/2002JD002066.

Barthe, C., W. Deierling, and M. C. Barth, 2010: Estimation of total lightning from various storm parameters: A cloud-resolving model study. *J. Geophys. Res.,* **115,** D24202, doi:10.1029/2010JD014405.

Blyth, A. M., H. J. Christian Jr., K. Driscoll, A. M. Gadian, and J. Latham, 2001: Determination of ice precipitation rates and thunderstorm anvil ice contents from satellite observations of lightning. *Atmos. Res.,* **59–60,** 217–229, doi:10.1016/S0169-8095(01)00117-X.

Boccippio, D. J., W. J. Koshak, and R. J. Blakeslee, 2002: Performance assessment of the Optical Transient Detector and Lightning Imaging Sensor. Part I: Predicted diurnal variability. *J. Atmos. Oceanic Technol.,* **19,** 1318–1332, doi:10.1175/1520-0426(2002)019<1318:PAOTOT>2.0.CO;2.

Cecil, D. J., S. J. Goodman, D. J. Boccippio, E. J. Zipser, and S. W. Nesbitt, 2005: Three years of TRMM precipitation features. Part I: Radar, radiometric, and lightning characteristics. *Mon. Wea. Rev.,* **133,** 543–566, doi:10.1175/MWR-2876.1.

——, D. E. Buechler, and R. J. Blakeslee, 2014: Gridded lightning climatology from TRMM-LIS and OTD: Dataset description. *Atmos. Res.,* **135–135,** 404–414, doi:10.1016/j.atmosres.2012.06.028.

Christensen, J. H., and Coauthors, 2007: Regional climate projections. *Climatic Change 2007: The Physical Science Basis,* S. Solomon et al., Eds., Cambridge University Press, 847–940.

Christian, H. J., and Coauthors, 2003: Global frequency and distribution of lightning as observed from space by the Optical Transient Detector. *J. Geophys. Res.,* **108,** 4005, doi:10.1029/2002JD002347.

Deierling, W., J. Latham, W. A. Petersen, S. M. Ellis, and H. J. Christian Jr., 2005: On the relationship of thunderstorm ice hydrometeor characteristics and total lightning measurements. *Atmos. Res.,* **76,** 114–126, doi:10.1016/j.atmosres.2004.11.023.

——, W. A. Petersen, J. Latham, S. Ellis, and H. J. Christian, 2008: The relationship between lightning activity and ice fluxes in thunderstorms. *J. Geophys. Res.,* **113,** D15210, doi:10.1029/2007JD009700.

Donner, L. J., and Coauthors, 2011: The dynamical core, physical parameterizations, and basic simulation characteristics of the atmospheric component AM3 of the GFDL Global Coupled Model CM3. *J. Climate,* **24,** 3484–3519, doi:10.1175/2011JCLI3955.1.

Dufresne, J. L., and Coauthors, 2013: Climate change projections using the IPSL-CM5 Earth System Model: from CMIP3 to CMIP5. *Climate Dyn.,* **40,** 2123–2165, doi:10.1007/s00382-012-1636-1.

Fiore, A. M., and Coauthors, 2012: Global air quality and climate. *Chem. Soc. Rev.,* **41,** 6663–6683, doi:10.1039/C2CS35095E.

Flannigan, M. D., M. A. Krawchuk, W. J. de Groot, B. M. Wotton, and L. M. Gowman, 2009: Implications of changing climate for global wildland fire. *Int. J. Wildland Fire,* **18,** 483–507, doi:10.1071/WF08187.

Gent, P. R., and Coauthors, 2011: The Community Climate System Model Version 4. *J. Climate,* **24,** 4973–4991, doi:10.1175/2011JCLI4083.1.

Grewe, V., D. Brunner, M. Dameris, J. L. Grenfell, R. Hein, D. Shindell, and J. Staehelin, 2001: Origin and variability of upper tropospheric nitrogen oxides and ozone at northern mid-latitudes. *Atmos. Environ.,* **35,** 3421–3433, doi:10.1016/S1352-2310(01)00134-0.

Huffman, G. J., R. F. Adler, D. T. Bolvin, and G. Gu, 2009: Improving the global precipitation record: GPCP Version 2.1. *Geophys. Res. Lett.,* **36,** L17808, doi:10.1029/2009GL040000.

Kloster, S., and Coauthors, 2010: Fire dynamics during the 20th century simulated by the Community Land Model. *Biogeosciences,* **7,** 1877–1902, doi:10.5194/bg-7-1877-2010.

Kummerow, C., and Coauthors, 2000: The status of the Tropical Rainfall Measuring Mission (TRMM) after two years in orbit. *J. Appl. Meteor.,* **39,** 1965–1982, doi:10.1175/1520-0450(2001)040<1965:TSOTTR>2.0.CO;2.

Lamarque, J.-F., and Coauthors, 2010: Historical (1850–2000) gridded anthropogenic and biomass burning emissions of reactive gases and aerosols: Methodology and application. *Atmos. Chem. Phys.,* **10,** 7017–7039, doi:10.5194/acp-10-7017-2010.

Lay, E. H., R. H. Holzworth, C. J. Rodger, J. N. Thomas, O. Pinto, and R. L. Dowden, 2004: WWLL global lightning detection system: Regional validation study in Brazil. *Geophys. Res. Lett.,* **31,** L03102, doi:10.1029/2003GL018882.

Lebsock, M., H. Morrison, and A. Gettelman, 2013: Microphysical implications of cloud-precipitation covariance derived from satellite remote sensing. *J. Geophys. Res. Atmos.,* **118,** 6521–6533, doi:10.1002/jgrd.50347.

Levy, H., II, W. J. Moxim, and R. S. Kasibhatla, 1996: A global three-dimensional time-dependent lightning source of tropospheric NO_x. *J. Geophys. Res.,* **101,** 22 911–22 922, doi:10.1029/96JD02341.

Li, F., X. D. Zeng, and S. Levis, 2012: A process-based fire parameterization of intermediate complexity in a Dynamic Global Vegetation Model. *Biogeosciences,* **9,** 2761–2780, doi:10.5194/bg-9-2761-2012.

Liu, C., D. Cecil, and E. J. Zipser, 2011: Relationships between lightning flash rates and passive microwave brightness temperatures at 85 and 37 GHz over the tropics and subtropics. *J. Geophys. Res.,* **116,** D23108, doi:10.1029/2011JD016463.

Mach, D. M., H. J. Christian, R. J. Blakeslee, D. J. Boccippio, S. J. Goodman, and W. L. Boeck, 2007: Performance assessment of the Optical Transient Detector and Lightning Imaging Sensor. *J. Geophys. Res.,* **112,** D09210, doi:10.1029/2006JD007787.

Meehl, G. A., and Coauthors, 2012: Climate system response to external forcings and climate change projections in CCSM4. *J. Climate,* **25,** 3661–3683, doi:10.1175/JCLI-D-11-00240.1.

Nesbitt, S. W., E. J. Zipser, and D. J. Cecil, 2000: A census of precipitation features in the tropics using TRMM: Radar, ice scattering, and lightning observations. *J. Climate,* **13,** 4087–4106, doi:10.1175/1520-0442(2000)013<4087:ACOPFI>2.0.CO;2.

Orville, R. E., G. R. Huffines, W. R. Burrows, and K. L. Cummins, 2011: The North American Lightning Detection Network (NALDN)—Analysis of flash data: 2001–09. *Mon. Wea. Rev.,* **139,** 1305–1322, doi:10.1175/2010MWR3452.1.

Papadopoulos, A., T. G. Chronis, and E. N. Anagnostou, 2005: Improving convective precipitation forecasting through assimilation of regional lightning measurements in a mesoscale model. *Mon. Wea. Rev.,* **133,** 1961–1977, doi:10.1175/MWR2957.1.

Pechony, O., and D. T. Shindell, 2009: Fire parameterization on a global scale. *J. Geophys. Res.,* **114,** D16115, doi:10.1029/2009JD011927.

Pessi, A. T., and S. Businger, 2009: Relationships among lightning, precipitation, and hydrometeor characteristics over the North Pacific Ocean. *J. Appl. Meteor. Climatol.,* **48,** 833–848, doi:10.1175/2008JAMC1817.1.

Petersen, W. A., and S. A. Rutledge, 1998: On the relationship between cloud-to-ground lightning and convective rainfall. *J. Geophys. Res.,* **103,** 14 025–14 040, doi:10.1029/97JD02064.

——, H. J. Christian, and S. A. Rutledge, 2005: TRMM observations of the global relationship between ice water content and lightning. *Geophys. Res. Lett.,* **32,** L14819, doi:10.1029/2005GL023236.

Pohjola, H., and A. Mäkelä, 2013: The comparison of GLD360 and EUCLID lightning location systems in Europe. *Atmos. Res.,* **123,** 117–128, doi:10.1016/j.atmosres.2012.10.019.

Price, C., 2009: Will a drier climate result in more lightning? *Atmos. Res.,* **91,** 479–484, doi:10.1016/j.atmosres.2008.05.016.

——, and D. Rind, 1992: A simple lightning parameterization for calculating global lightning distributions. *J. Geophys. Res.,* **97,** 9919–9933, doi:10.1029/92JD00719.

——, and ——, 1993: What determines the cloud-to-ground lightning fraction in thunderstorms? *Geophys. Res. Lett.,* **20,** 463–466, doi:10.1029/93GL00226.

——, and ——, 1994: The impact of a $2 \times CO_2$ climate on lightning-caused fires. *J. Climate,* **7,** 1484–1494, doi:10.1175/1520-0442(1994)007<1484:TIOACC>2.0.CO;2.

——, J. Penner, and M. Prather, 1997: NO_x from lightning: 1. Global distribution based on lightning physics. *J. Geophys. Res.,* **102,** 5929–5941, doi:10.1029/96JD03504.

Randall, D. A., and Coauthors, 2007: Climate models and their evaluation. *Climate Change 2007: The Physical Science Basis,* S. Solomon et al., Eds., Cambridge University Press, 589–662.

Said, R. K., U. S. Inan, and K. L. Cummins, 2010: Long-range lightning geolocation using a VLF radio atmospheric waveform bank. *J. Geophys. Res.,* **115,** D23108, doi:10.1029/2010JD013863.

——, M. B. Cohen, and U. S. Inan, 2013: Highly intense lightning over the oceans: Estimated peak currents from global GLD360 observations. *J. Geophys. Res. Atmos.,* **118,** 6905–6915, doi:10.1002/jgrd.50508.

Saunders, C. P. R., W. D. Keith, and R. P. Mitzeva, 1991: The effect of liquid water on thunderstorm charging. *J. Geophys. Res.,* **96,** 11 007–11 017, doi:10.1029/91JD00970.

Shindell, D. T., G. Faluvegi, N. Unger, E. Aguilar, G. A. Schmidt, D. M. Koch, S. E. Bauer, and R. L. Miller, 2006: Simulations of preindustrial, present-day, and 2100 conditions in the NASA GISS composition and climate model G-PUCCINI. *Atmos. Chem. Phys.,* **6,** 4427–4459, doi:10.5194/acp-6-4427-2006.

Stocker, T. F., and Coauthors, 2013: *Climate Change 2013: The Physical Science Basis.* Cambridge University Press, 1535 pp. [Available online at www.climatechange2013.org/images/report/WG1AR5_ALL_FINAL.pdf.]

Takahashi, T., 1978: Riming electrification as a charge generation mechanism in thunderstorms. *J. Atmos. Sci.,* **35,** 1536–1548, doi:10.1175/1520-0469(1978)035<1536:REAACG>2.0.CO;2.

Tapia, A., J. A. Smith, and M. Dixon, 1998: Estimation of convective rainfall from lightning observations. *J. Appl. Meteor.,* **37,** 1497–1509, doi:10.1175/1520-0450(1998)037<1497:EOCRFL>2.0.CO;2.

Taylor, K. E., R. J. Stouffer, and G. A. Meehl, 2012: An overview of CMIP5 and the experiment design. *Bull. Amer. Meteor. Soc.,* **93,** 485–498, doi:10.1175/BAMS-D-11-00094.1.

Thonicke, K., A. Spessa, I. C. Prentice, S. P. Harrison, L. Dong, and C. Carmona-Moreno, 2010: The influence of vegetation, fire spread and fire behaviour on biomass burning and trace gas emissions: Results from a process-based model. *Biogeosciences,* **7,** 1991–2011, doi:10.5194/bg-7-1991-2010.

Tost, H., P. Jöckel, and J. Lelieveld, 2007: Lightning and convection parameterisations—Uncertainties in global modelling. *Atmos. Chem. Phys.,* **7,** 4553–4568, doi:10.5194/acp-7-4553-2007.

Vecchi, G. A., and B. J. Soden, 2007: Global warming and the weakening of the tropical circulation. *J. Climate,* **20,** 4316–4340, doi:10.1175/JCLI4258.1.

Virts, K. S., J. M. Wallace, M. L. Hutchins, and R. H. Holzworth, 2013: Highlights of a new ground-based, hourly global lightning climatology. *Bull. Amer. Meteor. Soc.,* **94,** 1381–1391, doi:10.1175/BAMS-D-12-00082.1.

Williams, E. R., 2005: Lightning and climate: A review. *Atmos. Res.,* **76,** 272–287, doi:10.1016/j.atmosres.2004.11.014.

——, and S. Stanfill, 2002: The physical origin of the land–ocean contrast in lightning activity. *C. R. Phys.,* **3,** 1277–1292, doi:10.1016/S1631-0705(02)01407-X.

——, and Coauthors, 2002: Contrasting convective regimes over the Amazon: Implications for cloud electrification. *J. Geophys. Res.,* **107,** 8082, doi:10.1029/2001JD000380.

Wu, S., L. J. Mickley, D. J. Jacob, D. Rind, and D. G. Streets, 2008: Effects of 2000–2050 changes in climate and emissions on global tropospheric ozone and the policy-relevant background surface ozone in the United States. *J. Geophys. Res.,* **113,** D18312, doi:10.1029/2007JD009639.

Wu, T., and Coauthors, 2010: The Beijing Climate Center atmospheric general circulation model: Description and its performance for the present-day climate. *Climate Dyn.,* **34,** 123–147, doi:10.1007/s00382-008-0487-2.

Zipser, E. J., C. Liu, D. J. Cecil, S. W. Nesbitt, and D. P. Yorty, 2006: Where are the most intense thunderstorms on Earth? *Bull. Amer. Meteor. Soc.,* **87,** 1057–1071, doi:10.1175/BAMS-87-8-1057.